In this study, a large-scale magnetic rotator for hydrogen production boosting was designed. The study addresses the challenge of selecting and designing mechanical components for a dynamic magnetic field (DMF) magnetic rotator in a green hydrogen electrolysis power plant, focusing on ensuring component reliability and efficiency under operational stresses. The aim is to determine suitable machine element materials (shaft, clutch, gears, etc.), allowable shear stress, and interconnection mechanisms through theoretical and practical evaluations. The method includes calculating the allowable shear stress for the spline based on carbon steel tensile strength, applying safety factors for material properties and load considerations, and determining shaft diameter using torque and shock load factors. Standard catalogs guide the selection of interconnections like clutches, gears, and bearings to ensure compatibility and performance. The results indicate that a 95 mm diameter S30C carbon steel shaft, with an allowable shear stress of 7.8 kg/mm^2, meets the design requirements. The chosen spline dimensions and a 12.5 MW, 14-pole induction motor align with the system's needs, ensuring reliable operation. The discussion highlights the critical balance between theoretical predictions and practical application in design optimization. It underscores the importance of incorporating safety factors and verifying component suitability to ensure robust performance of the magnetic rotator. This study provides a comprehensive approach to design optimization, integrating theoretical analysis with practical considerations to achieve optimal performance and reliability. The design output of this study can be used to boost the hydrogen evolution reaction in the SIEMENS Sylizer 300 electrolysis cell

Keywords: magnetic rotator, green water electrolysis, hydrogen production, design optimization

UDC 6.620.3
DOI: 10.15587/1729-4061.2024.308944

DEVELOPMENT OF A MAGNETIC ROTATOR TO ENHANCE THE HYDROGEN EVOLUTION REACTION IN A PROTON EXCHANGE MEMBRANE WATER ELECTROLYSIS CELL

Purnami Purnami
Doctor of Engineering, Associate Professor*
Willy Satrio Nugroho
Doctor of Engineering, Assistant Professor*
Lukman Hakim
Doctor of Engineering, Associate Professor
Department of Chemistry**
I Nyoman Gede Wardana
Corresponding author
Doctor of Engineering, Professor*
E-mail: wardana@ub.ac.id
*Department of Mechanical Engineering**
**Brawijaya University
M. T. Haryono str., 167, Malang, Indonesia, 65145

Received date 11.07.2024
Accepted date 13.09.2024
Published date 25.10.2024

How to Cite: *Purnami, P., Nugroho, W. S., Hakim, L., Wardana, I. N. G. (2024). Development of a magnetic rotator to enhance the hydrogen evolution reaction in a proton exchange membrane water electrolysis cell. Eastern-European Journal of Enterprise Technologies, 5 (1 (131)), 6–16. https://doi.org/10.15587/1729-4061.2024.308944*

1. Introduction

Green water electrolysis holds the promise to make a sustainable future of energy. Green hydrogen promises that the net zero emission (NZE) goal stated in the Paris Climate Agreement will be achieved by 2050 [1]. The term green hydrogen comes from the hydrogen color spectrum classification based on carbon footprints [2]. Green hydrogen is hydrogen produced through zero carbon emission, such as water electrolysis with renewable electricity sources. Grid sourced electrolysis does not belong to green hydrogen due to moderate carbon footprint, so it is classified as yellow hydrogen [3]. Nuclear sourced electrolysis or nuclear-hydrogen cogeneration plant falls into the pink hydrogen color spectrum, because even though it has a zero carbon footprint, it poses security risks due to nuclear energy usage [4]. When the carbon byproduct is not in the form of CO_2, such as in methane pyrolysis, the color code is turquoise [5]. Therefore, the study to generate the design of a mechanical system to support green hydrogen production boosting is urgently needed.

Many technical challenges in green water electrolysis technologies still exist and need to be tackled. The main problem is the low efficiency of electrolysis cells and the involvement of noble catalyst material [6]. There is a tradeoff between cell technology and the cost of hydrogen fuel production. Sophisticated cell technology will result in high hydrogen prices per kilogram while the conventional technology has low efficiency (about 67 %) [7]. Currently, the smallest hydrogen price per kilogram is still higher than the average gasoline, which is $3.00/kg compared to $1.50/kg [8]. Hence, most of the current hydrogen production is through methane steam reforming, classified as brown hydrogen [9]. Therefore, a study to reports the design optimization of an extension technology to boost hydrogen production from water electrolysis based on the main paradigm of giving external disruption to allow rapid ionization of water is required.

2. Literature review and problem statement

The paper discusses the breakthrough in improving the efficiency of electrolysis cells through external magnetic field exposure (EMF). The EMF leverages the magnetic susceptibility of water molecules due to their fully filled molecular orbitals. The electron pair in the water's molecular orbital aligns the spin pair from the para state (bidirectional state with reverse direction +1/2 and −1/2) to the ortho state (unidirectional state) [10]. Consequently, the water molecule moves away from the EMF source to restore the bidirectional spin pair through entanglement, adhering to the energy minima principle [11]. Since the water molecules do not move far enough from the EMF source, the ortho state persists. In the ortho state, the electron pairs in both O-H bonds are unstable due to their alignment in the same direction, causing the hydrogen atoms to repel each other and resulting in a less stable O-H bond compared to para water [12]. The simplest method to achieve this condition is by placing a pair of magnets around the cathode, exerting Lorentz force towards the diffusion layer [13]. The effect was improved by rotating one of the magnets around the electrode, which increases the hydrogen evolution reaction (HER) up to 2 times [14]. Further improvement of dynamic magnetic field (DMF) assisted electrolysis was by making the rotational speed of the system adjustable, which improved the total efficiency and HER of the system by 2.5 times from the initial condition [15]. Another approach to improving HER is by introducing chaos in the diffusion layer, which increases the collision chance during Brownian motion [16]. Several ways to control motion in the diffusion layer are available. One example is through micelles formation by employing surfactants [17]. But there are still unresolved questions related to the practical implementation and scalability of this technology. The reasons for these unresolved issues may be that the alignment of electron pairs from the para state to the ortho state in water molecules requires precise control, which is challenging to maintain consistently across large-scale systems. There might be fundamental limits to how much the EMF can enhance HER, particularly in terms of the stability of the ortho state of water molecules under prolonged exposure. Implementing dynamic magnetic field (DMF) systems involves significant costs, especially considering the materials and machinery required to generate and maintain the magnetic fields.

An option to overcome these difficulties can be the development of more sophisticated control systems for EMF exposure, using materials with better magnetic and electrical properties, and exploring cost-effective materials and scalable designs. The concrete machine design concept for DMF has to concern the relationship between the design concept and material requirements. The performance of a newly designed product largely depends on the absorptive capacity [18]. This is related to the material selection process where the chosen material has to fit the purposes of the design. For example, special treatment has to be applied to improve the biocompatibility of AISI316L steel for medical applications through chitosan immersion [19]. Another example is the use of Epoxy-FeNdB-Mn, applied to absorb electromagnetic waves, which is useful in radar avoidance [20]. In general, surface treatment such as surface roughness control and paint is effective to inhibit corrosion, making the product more durable [21]. Surface roughness can be controlled during machining by setting correct parameters such as cutting direction in milling [22]. Another way to improve durability and wear resistance is by other material coating, such as fiberglass coating, which shows a great strength resistance [23]. Furthermore, the quality of the material throughout the application can be examined during processing and post-application, for example, using the Taguchi method, Promethee, or other design of experiment techniques [24, 25]. In this study, the scope of the design is on the machine element design and material selection, which is essential to provide an effective DMF rotator.

The design in this work is specific for the SIEMENS Silyzer 300 proton exchange membrane (PEM) water electrolysis cell. The Siemens Silyzer 300 is a PEM electrolyzer designed for efficient hydrogen production through water electrolysis [26]. The core of the system features a series of PEM cells, where water is split into hydrogen and oxygen using electricity via an iridium (II) oxide anode (IrO_2) and platinum (Pt) cathode. IrO_2 is used as an anode material due to its conductivity, stability, durability, and corrosion resistance [27]. Pt was chosen as the cathode material due to its high electron density, representing its capability to deliver high amounts of current density [28]. The design emphasizes high efficiency, compact footprint, and scalability, allowing multiple units to be combined for increased hydrogen output in few stacks [29]. Each cell contains a proton-conducting membrane sandwiched between two electrodes, with water supplied to the anode where it splits into oxygen, protons, and electrons. The protons move through the membrane to the cathode, where they combine with electrons to form hydrogen gas. Selective permeability of the membrane ensures efficient separation of hydrogen and oxygen gases and sustains the electrolytic process by facilitating continuous proton flow while maintaining electrical neutrality [30].

In this study, the principle of machine element design is used to design the magnetic rotator module. The principle of machine element design involves the systematic process of designing individual parts (elements) of a machine to perform specific functions within the overall mechanical system [31]. This process considers factors such as material selection, stress and strain analysis, load-bearing capacity, durability, manufacturability, and cost efficiency depends on the technology readiness level (TRL) target of the design [32]. This engineering principle is required to ensure that each machine element, such as gears, bearings, springs, and fasteners, meets the required performance standards and safety margins while optimizing longevity and reliability [33]. The goal is to create a cohesive and functional machine by integrating well-designed elements that work harmoniously under expected operating conditions. The aim of this study is to provide the design of the DMF rotator elements based on the target current density at the cathode.

This study pioneers the integration of DMF to enhance the HER rate, directly addressing the persistent challenge of low efficiency in conventional electrolysis cells, a problem widely recognized but not fully resolved in the existing literature. Previous studies have identified limitations in traditional electrolyzers, particularly in terms of inefficient electron transfer and water molecule dissociation, but they have not successfully tackled these issues in a scalable and sustainable manner. By designing a magnetic rotator module with a focus on optimizing material selection and structural integrity, this research proposes a novel solution to improve system performance. The innovative DMF rotator's ability to manipulate water molecule states and enhance electron spin alignment offers a promising approach to overcoming these efficiency barriers. This marks the first attempt to optimize

the design based on electron target velocity, presenting a substantial advancement in electrolysis technology. The solution not only aims to improve efficiency but also contributes to sustainability goals, addressing the larger unresolved problem of reducing carbon emissions. Grounded in machine element design principles, this comprehensive methodology ensures practical applicability and reliability, offering a significant step toward scalable and sustainable energy solutions. The aim of this study follows logically from the broader unresolved issue of inefficient electrolysis, making it a promising direction for future research.

All this allows us to assert that it is expedient to conduct a study on integrating a DMF-based magnetic rotator to enhance the HER rate. Given the persistent inefficiencies in conventional electrolysis systems, particularly related to suboptimal electron transfer and water dissociation, this research direction is justified by the need for a scalable and sustainable solution. The design optimization of the rotator, based on material selection and electron velocity targeting, promises to address these inefficiencies while contributing to the broader goal of reducing carbon emissions and advancing renewable energy technologies.

3. The aim and objectives of the study

The aim of the study is to provide a design optimization of the magnetic rotator to support a large-scale DMF module to be used in the SIEMENS Sylizer 300 PEM electrolyzer. This will make it possible to double the hydrogen production rate of the SIEMENS Sylizer 300 electrolyzer.

To achieve this aim, the following objectives are accomplished:

– to perform a conceptual design of the magnetic rotator based on the electron density in the cathode of the SIEMENS Sylizer 300 PEM electrolyzer;

– to perform the determination of mechanical parts and interconnection based on the conceptual design;

– to perform the selection of mechanical elements for each part based on the allowable mechanical stresses.

4. Materials and methods

The research object of this study is the Dynamic Magnetic Field (DMF) magnetic rotator, designed to enhance hydrogen production in the SIEMENS Sylizer 300 electrolysis cell by optimizing magnetic field interactions with the cathode. The main hypothesis of this study is that by designing and implementing a modular DMF magnetic rotator, the magnetic field will significantly enhance electron velocity, improve current distribution, and optimize the hydrogen evolution reaction (HER) in the water electrolysis process.

The theoretical methods chosen for this study are based on the well-established first principle of the magnetic theorem, which is the Lorentz force and its interaction with the electron affecting the electron velocity, both of which are critical to understanding the interaction between magnetic forces and the cathode during electrolysis. This introduces the current scale factor to ensure accurate scaling of the current distribution across the cathode, which is considered a key factor in uniform hydrogen production.

The conceptual design of the DMF magnetic rotator started from the target electron velocity. The rotator components have to cover the entire cathode plate area of the SIEMENS Sylizer 300 module. However, it is impossible to construct a 1:1 magnetic face since there are 24 modules of cathode and anode pairs on the stack. As a result, the design constraint is $L=H_m$ where L is the length of the magnets, and H_m is the height of the module, which is 4 m. The magnet strength was measured by Lorentz force using equation (1). The v symbol in equation (1) represents the electric current velocity while the electron velocity is v_e included in the current density equation in equation (2), which consists of the number of moles of the electrons (n), the Faraday constant (F) 96.485 C·mol^{-1}, and the area of the electrode (A). In equation (3), the moles of the electron are represented as the electric current over the charge. This information was useful to form equation (4) where the current scale factor (*ISF*) was introduced at the cathode so that *CD* is the cathode volume dimension. The scale factor can be depicted as the current spread all over the cathode to form the inner Helmholtz layer.

The design concept used to build the DMF magnetic rotator is a modular design concept. The modular design allows the part to be disassembled, which eases the displacement. The ease of displacement is considered to ease the maintenance operation when the magnets need to be replaced or cleaned. In this work, the magnets were neodymium N52 magnets with the dimension of 40×10×5 mm. The magnets were placed as an array with two sides (north and south) connected with a single plate in between of both sides. The connected modules were then placed on top of a block attached to the rotator shaft. The entire component was attached with fasteners. The total weight of the component was 629.0425 kg. The weight becomes the basis to choose the electric motor based on the operational power calculation using equation (5) and visually using the general motors (GM) chart:

$$F_L = q\left(v_e \times B\right), \tag{1}$$

$$j = nF_L A v_e, \tag{2}$$

$$n = \frac{I}{q}, \tag{3}$$

$$\frac{vB}{s} = CD \times n \times ISF, \tag{4}$$

$$P = \frac{\tau \times 2\pi \times \omega}{60}. \tag{5}$$

Formulas (1)–(5) use the following symbols:
– F_L – Lorentz force (N);
– q – charge at the cathode (C);
– v_e – current speed at the cathode (m·s^{-1});
– j – current density (A·ms^{-2});
– A – electrode area (m^2);
– I – amount of current (A);
– B – magnetic field strength (T);
– CD – cathode volume dimension (m^3);
– n – current carried by the electron (A·C^{-1});
– ISF – current scale factor;
– s – magnetic field exposure time (s);
– P – mechanical power (W);
– τ – torsion (N·m);
– ω – DMF rotational speed (RPM).

Determining the mechanical parts of DMF magnetic rotators involves identifying and understanding the components. The flow of the design performed in this work follows the

machine design principle by [34]. The process started with a detailed review of design schematics, technical drawings, or exploded view diagrams showing the arrangement and interaction of each part. Key parts such as gears, bearings, shafts, springs, and fasteners are identified by their specific functions and physical characteristics. The parts catalogs, specifications, and standards to ensure that each component meets the required dimensions, materials, and tolerances are obtained from machine design algorithms for each specific part [34]. The general flow of the design is provided in Fig. 1 as a flowchart.

The DMF magnetic rotator design process began with designing the system, including the rotor and stator components, specifying dimensions, materials, and placement of magnets. The material selection process was mainly based on the allowable stress. The rotor was constructed by evenly attaching magnets on two sides ensuring correct orientations of the north and south poles and securing them with fasteners. The rotator was assembled by mounting the rotor on a freely spinning shaft and positioning the cathode close to the rotor magnets without contact. Electrical connections were made to an external power source or control circuit to manage rotation speed and direction. The system was tested and calibrated by applying fixed rotational speed and control to 500 RPM [35]. Safety and maintenance checks were conducted to ensure secure electrical connections, regular inspections, and maintenance of the magnets and coils.

The DMF magnetic rotator utilized a motor as the primary power source, requiring secure mounting for stable operation. A clutch mechanism was then introduced to regulate torque transmission between the motor and the drive shaft. The drive shaft itself facilitated power transfer and required a bearing for smooth rotation at its designated location. The pinion gear, fixed to the drive shaft, served to increase rotational speed by meshing with a larger gear. The counterpart to the pinion gear was the spiral bevel ring gear, designed to transmit rotational power at 90° (transmit horizontal to vertical). This ring gear was mounted on a separate frame for proper alignment and meshing with the pinion gear. The system was also designed to be modular, so it can be organized as a stack similar to the SIEMENS Sylizer 300 PEM stack. The main parts of each DMF rotator module can be seen in Fig. 2.

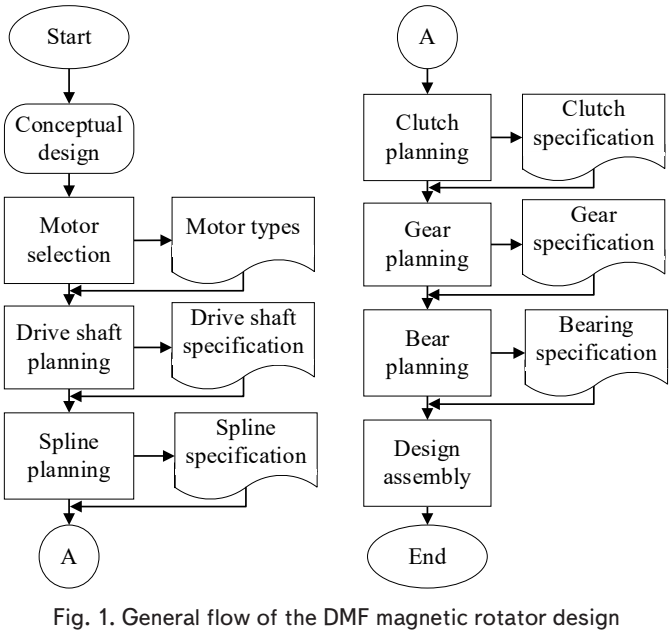

Fig. 1. General flow of the DMF magnetic rotator design

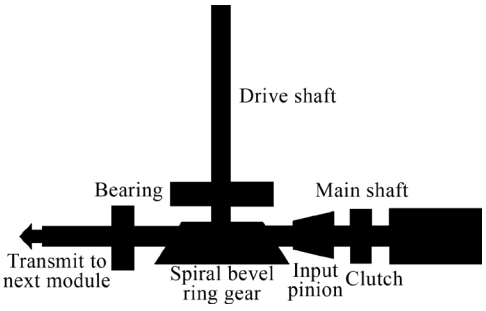

Fig. 2. Machine elements involved in the core design of the DMF magnetic rotator

The assembly process involved sequential mounting of the motor on a stable base, followed by clutch attachment according to the manufacturer's specifications. The drive shaft received a bearing for smooth rotation, and the pinion gear was secured using appropriate locking mechanisms. The spiral bevel ring gear was then mounted on a separate frame, meticulously aligned with the pinion gear for optimal meshing. Finally, the drive shaft was connected to both gears, and the entire system underwent a no-load test run to verify proper functionality before application.

5. Results of dynamic magnetic field magnetic rotator design optimization

5. 1. Conceptual design results of the dynamic magnetic field magnetic rotator

The electric motor process is based on theoretical and actual visual techniques. The electric motor selections were likely driven by the need for both high power output and a moderate rotational speed of 500 rpm. According to the selection chart in Fig. 3, this combination points towards a motor with a lower number of poles – 14. A lower pole count aligns with the ability to deliver the required power at the desired speed. The number of poles in an electric motor influences its torque, efficiency, size, weight, and application suitability [36]. Motors with more poles generally produce higher torque due to increased magnetic interactions per revolution, making them ideal for high-torque, low-speed applications such as conveyors and crushers. In contrast, motors with fewer poles are more efficient at higher speeds and are typically used in applications like fans and pumps. This is the reason to choose 14 poles for the DMF magnetic motor. Additionally, motors with more poles tend to be larger and heavier because they require more winding turns and magnetic materials, impacting their overall design and integration into the system.

The theoretical result is 13 MW operation power, which comes from equation (5) considering the machine's rotational speed (RPM) and torque (Nm). The calculation multiplies torque by a constant and speed (converted to seconds) to find theoretical rotational work output, then divides by another conversion factor to express it as power (watts). The theoretical value of 13 MW does not represent the actual work that can be supported by the motor. However, the technology of a 14-pole induction motor specified by the vendor ensures that the 13 MW theoretical work can be covered by a 12.5 MW motor. Therefore, we choose the 12.5 MW 14-pole high-speed induction motor for the power source of the system.

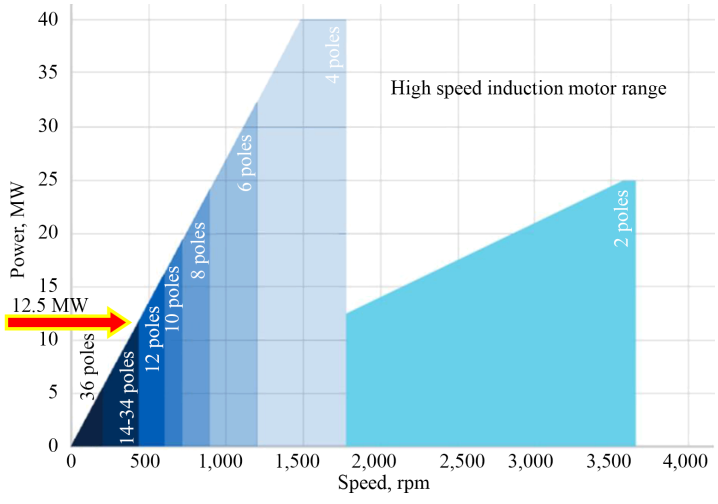

Fig. 3. Machine elements involved in the core design of the DMF magnetic rotator

5. 2. Results of parts and interconnection determination

To determine the shaft material and the allowable shear stress for the spline in the DMF magnetic rotator, we use equation (6). Here, σ_b represents the tensile strength of the chosen shaft material, which in this case is SC steel with a tensile strength of 58 kg/mm^2. The safety factor for the material (SF1) is set at 6.0, considering the inherent properties and expected loads on the material. Additionally, a safety factor of 1.3 (SF2) is applied due to the absence of a keyway, which influences the overall safety margin. By dividing the tensile strength by the product of these safety factors, we determine the allowable shear stress for the spline to be 7.8 kg/mm^2. This calculation ensures that the shaft material will perform reliably under the operational stresses encountered in the magnetic rotator, maintaining structural integrity and safety. To determine the shaft diameter (d_s) for the DMF magnetic rotator, we use equation (7). The coefficient (C_b) is 1.0, indicating no bending load. The torque (T) applied to the shaft is 430542 kg·mm, the shock load factor (K_T) is 3.0, accounting for the impact or shock loads on the shaft. Rounding up to the nearest standard size from the result, the shaft diameter is determined to be 95 mm. This calculation ensures that the shaft can handle the specified torque and shock loads without exceeding the allowable shear stress, providing a safe and reliable design for the magnetic rotator. To verify the shear stress on the shaft for the DMF magnetic rotator, we use equation (8). The calculated shear stress of approximately 2.6 kg/mm^2 confirms that it is well within the allowable shear stress of 7.8 kg/mm^2. This means that the shaft is suitably designed to handle the applied torque without exceeding the material's shear capacity, ensuring safe and reliable operation in the magnetic rotator:

$$\tau_a = \frac{\sigma_b}{SF1 \times SF2}, \tag{6}$$

$$d_s = \left(\frac{5.1}{\tau_a} \times K_T \times C_b \times T\right)^{1/3}, \tag{7}$$

$$\tau = \frac{5.1T}{d_s^3}. \tag{8}$$

Formulas (6)–(8) use the following symbols:
– τ_α – allowable shear stress (kg·mm^{-2});
– σ_b – tensile strength (kg·mm^{-2});
– $SF1$ – safety factor 1;
– $SF2$ – safety factor 2;
– d_s – shaft diameter (mm);
– C_b – bending load coefficient;
– T – applied torque (kg·mm);
– CD – cathode volume dimension (m^3);
– K_T – shock load factor;
– τ – shear stress (kg·mm^{-2}).

The selection of the appropriate spline for the shaft in the DMF magnetic rotator is essential to ensure that the chosen spline can handle the applied forces without exceeding the material's shear capacity. Given the shaft diameter (d_s) of 95 mm, we have two options for spline sizes: one with dimensions l=80–320 mm and b=28 mm. To determine the force (F) acting on the spline, we use equation (9). This calculated shear stress of 2.28 kg/mm^2 determined using equation (10) is well within the allowable limits, indicating that the selected spline dimensions are suitable for handling the applied torque without exceeding the material's shear capacity, thus ensuring reliable and safe operation in the magnetic rotator:

$$F = \frac{2T}{d_s}, \tag{9}$$

$$\tau_s = \frac{F}{bl}. \tag{10}$$

Formulas (9), (10) use the following symbols:
– F – force acting on the spline (kg·mm^{-2});
– T – torque applied on the spline (kg·mm);
– d_s – shaft diameter (mm);
– b – spline cross-section (mm);
– l – spline length (mm);
– τ_s – shear stress (kg·mm^{-2}).

The magnitude and type of the main stress applied to the system were determined. Consequently, the interconnection to provide power transmission in the system can be determined using the standard parts. The interconnections are the clutch, gears, and bearings. The clutch between the main shaft and the motor is essential to provide extra protection during operation. We found that the fixed clutch is useful to hold the main shaft to the motor spindle, which can be held using flanges with the standard fastener diameter of M25. The chosen gear set required to transmit power from horizontal to vertical arrangement is a 1:1 ratio spiral bevel ring gear arranged in millet. The bearing has to handle 630 kg working weight, which is classified as a high load. Therefore, the needle roller bearing type is chosen over the ball bearing.

5. 3. Results of mechanical elements selection for the DMF magnetic rotator

The main parts selection is the shaft to transmit the power from the motor and hold other elements. This shaft features a solid round design with a diameter of 95 mm. This critical dimension dictates the shaft's strength and its ability to handle loads. The chosen material is S30C carbon steel, which is a common choice for its affordability, good machinability, and adequate strength, making the shaft a practical solution for various applications [37]. The design incorporates a bearing placement strategically positioned 4200 mm from a reference point located about the end of the shaft. The placement information is vital for calculating the bending moments and forces acting on the shaft, especially around the bearing location [38]. The shaft has a spline for clutch interconnection. The spline

features a series of grooves or teeth machined directly onto the 95 mm diameter shaft [39]. These grooves interlock with corresponding teeth on a mating part, enabling relative axial movement (sliding) along the shaft while preventing unwanted rotation.

The technical parameters of the rotator before and after scaling up from lab scale to large scale demonstrate significant improvements in performance and design. The side by side comparison of the DMF rotator on a lab scale and the scaled-up version is listed in Table 1. Initially, the lab-scale rotator with a lower power capacity suffered from material inadequacies, particularly in handling working stress, which makes it unsuitable to directly handle prolonged workloads. The use of standard steel for the rotator material and a smaller shaft diameter (<50 mm) limited its ability to manage torque and operational loads effectively. After scaling up, the system incorporates a 12.5 MW power capacity, a 95 mm S30C carbon steel shaft, and a suite of optimized components, including an M25 fixed coupling, S45C carbon steel gears, and NA6917 needle roller bearings. These upgrades, along with an increased safety factor and higher allowable shear stress, ensure reliable operation under industrial-scale conditions. The enhanced material selection and increased load-handling capacity ensure robust performance, aligning the system with the operational demands of the larger Siemens Sylizer 300 PEM electrolyzer.

The magnetic holder has a critical role to secure the placing of the large-scale magnet. The holder design objective is to survive high shear stress and rotation forces while in operation. The holder design in the model of the scaled-up version of DMF is shown in Fig. 4. The main goal of the holder is to keep the magnet steady in its original position and orientation for safety and performance reasons during operation. The main design of the holder has ensured that the material was tough and precisely engineered to withstand greater mechanical stresses resulting from continuous operation, estimated for 10 hours.

Table 1

Comparison of technical parameters before and after scaling up

Parameter	Before improvement (lab scale)	After improvement (large scale)	Improvements
Rotator power capacity (MW)	Small power <100 W	12.5 MW	Power scaled up to meet industrial demand
Rotator material	Standard Steel (not selected wisely)	S30C Carbon Steel (selected wisely)	Chosen based on working stress and durability
Shaft diameter (mm)	Smaller, e.g., 50 mm	95 mm	Increased to handle higher torque and stress loads
Rotational speed (RPM)	Not carefully calculated prior to implementation	Specifically designed for 500 RPM	Adapted to the larger motor requirements
Allowable shear stress (MPa)	Lower stress tolerance	Higher, based on S30C	Materials chosen for higher load capacity
Bearing type and model	–	NA6917 Needle Roller Bearings	Improved for durability under heavy loads
Coupling type	–	M25 Fixed Coupling	Designed for enhanced power transmission
Gear material	–	S45C Carbon Steel Gears	Selected for strength and wear resistance
Safety factor	Undetermined	>1.5	Increased for safe operation under larger loads
Load handling (N·m)	Under 10 N·m	>500 N·m	Enhanced to accommodate the larger scale of operation
System complexity	Simple lab design	Industrial-scale system	Upgraded to handle operational complexities

The presence of a magnetic holder guarantees the overall performance stability and safety of such systems preventing any possible displacements or failures due to forces acting on the magnets. As such, it is a necessary upgrade that ensures operational integrity as well as long-term magnet stability within expanded systems.

Fig. 4. Model of the improved DMF rotator with the magnetic holder

The selection of the interconnection for the DMF magnetic rotator requires standard part selection from the catalogs. The standard catalog is the catalogs to choose parts or elements in which the dimension and design requirements are standard or available on the market [40]. The material selection for the clutch, gears, and bearings also includes the dimension selection based on the standard check. The standard check is the comparison of the maximum working stress with the allowable working stress [41]. The available material on the market for the M25 fixed coupling with flages is S30C carbon steel. The material for the gears has to be slightly stronger compared to the material of the shaft, which is S45C carbon steel. The needle roller bearing NA6917 is selected for the bearing to support the main shaft.

6. Discussion of the mechanical elements selection process for the DMF magnetic rotator

The proposed solutions successfully address the problem area,

which centered on inefficiencies in conventional electrolysis cell designs and material selection limitations in the lab-scale magnetic rotator. By scaling up the system, increasing the rotator power capacity to 12.5 MW, and optimizing material choices like S30C carbon steel for the shaft and S45C for the gears, the design overcomes previous inefficiencies and enhances load handling capabilities. The integration of higher shear stress tolerance and improvements in power transmission components such as bearings and couplings closes the gap between lab-scale shortcomings and industrial requirements. These modifications, systematically based on mechanical and operational demands, directly fulfill the research aim of improving efficiency, scalability, and durability in electrolysis systems. The evidence of increased power, stress resistance, and operational safety confirms the effectiveness of these solutions in closing the identified problem area.

The conceptual design transformed into technical specifications of the DMF magnetic rotator. Transforming a conceptual design into technical specifications involves translating broad ideas into detailed, actionable requirements [42]. The process starts with defining the project's scope, objectives, and constraints based on the initial concept. Following that, detailed drawings, schematics, and models were made to represent the design accurately. These are supplemented with precise measurements, materials specifications, and performance criteria, ensuring that the design meets regulatory standards and functional requirements. One of them is the safety factor, which is a must in every engineering design. In this design, the safety factor is multiplied by the maximum stress, which accounts to the maximum allowable stress tolerance. The safety factor is required to incorporate unexpected conditions such as uncertainty in materials and under/overload estimations [43].

The selection of the motor as a power source involves technical and scientific considerations. The motor is selected for applications requiring low-speed, high-torque performance due to their inherent design characteristics, which is aligned with 500 rpm rotational speed and 630 kg load. A higher number of poles reduces the synchronous speed, making them suitable for heavy-duty machinery where precise speed control at lower RPMs is essential [44]. Additionally, 14-pole motors offer better torque per ampere compared to motors with fewer poles, improving efficiency and reducing energy consumption in high-load scenarios [45]. However, there is a discrepancy in the conceptual selection between theoretical and visual GM chart methods. The theoretical method suggests a 30 MW 14-pole induction motor while the GM chart suggests a 25 MW 14-pole induction motor. The discrepancy could be due to several factors such as simplifications and empirical data involved in testing.

The design guideline takes into account mechanical stresses. In the design of the DMF shaft, tensile, compressive, shear, and bending stresses are considered. Tensile and compressive stresses occur when the shaft is subjected to axial forces, pulling or pushing along its length. Shear stress arises from forces acting parallel to the cross-section, such as torque transmitted by the shaft [46]. Bending stress occurs when transverse forces cause the shaft to bend, which is particularly significant at points of load application, such as where the bearing is positioned 4200 mm from the reference point. These stresses were carefully calculated to ensure that the shaft can handle the loads without exceeding the material's yield strength, which would lead to permanent deformation, or its ultimate strength, which would result in failure [47]. Improper material selection or design miscalculations could lead to fatigue, excessive deformation, or even catastrophic failure, compromising the entire mechanical system's performance and safety [48]. Using S30C carbon steel, known for its balance of strength and machinability, helps manage these stresses effectively.

The DMF magnetic rotator design directly applies the first principle of machine design. The concept of maximum allowable stress in machine design is rooted in material science and engineering principles. Maximum allowable stress is the highest stress that a material can withstand under operating conditions without failing [49]. This value is determined by dividing the material's yield strength or ultimate tensile strength by a safety factor. Yield strength is the stress at which a material begins to deform plastically, while ultimate tensile strength is the maximum stress a material can withstand before fracturing [50]. The application of the safety factor ensures that operational stress remains within a safe range, preventing plastic deformation and failure. The selection of the safety factor depends on the application, the consequences of failure, material properties, and the reliability of loading conditions. In critical applications where failure can result in significant consequences, for example, in a DMF magnetic rotator for a green hydrogen electrolysis power plant, a higher safety factor is required.

The interconnection mechanism in the design of the shaft involves the use of splines and couplings to transmit torque and ensure precise mechanical alignment. Splines are grooves or teeth machined directly onto the 95 mm diameter shaft, which interlock with corresponding teeth on a mating part, such as a clutch. This design ensures efficient torque transfer and maintaining the alignment of connected components. The use of a standard M25 fixed coupling with flanges made from S30C carbon steel facilitates secure attachment of the shaft to the fixed clutch. This coupling ensures that the rotational force is transmitted effectively without slippage. Slippage is an imperfect interlocking between two mechanical parts, which causes the existence of friction [51]. Friction could cause a thermal effect on the material, which changes the property of the material due to the high calorific value heat transfer in a perfect thermal contact [52]. As a result, the connected surface may contain many residual stresses, which weaken the connection. The material selection of gears with S45C ensures compatibility and sufficient strength to handle the applied loads. The needle roller bearing NA6917 supports the shaft, reducing friction and wear while accommodating radial loads, which is crucial for the shaft's stability and longevity. The integration of these components based on standard catalogs and maximum working stress checks ensures that the design is reliable, efficient, and meets industry standards for mechanical performance.

The main concept of DMF magnetic rotator design is that it depends on electron density at the cathode. Hence, the size consideration of the magnetic rotator is 1:1 to the size of the cathode. The study [49] considers only the allowable stress, which makes more design constraints applied to this study. The DMF design not only has to fulfill the maximum allowable stress tolerance but also has to be effective to support HER in the cathode. Compared to the study [51], which also includes friction, more constraints are applied in this study. As a result, the DMF design fulfills the performance and safety in [49] and [51] but also provides effectiveness for HER.

The Dynamic Magnetic Field (DMF) enhances the hydrogen evolution reaction (HER) by improving ion mobility

and mitigating electrode fouling. The rotating magnetic field introduces convective effects that reduce diffusion limitations, allowing hydrogen ions (H^+) to reach the cathode more efficiently and sustain higher reaction rates by minimizing concentration polarization. Additionally, the dynamic nature of the DMF prevents electrode fouling by displacing bubbles that accumulate on the cathode, maintaining prolonged electrode activity and ensuring consistent HER performance over time. DMF also affects water molecules due to their diamagnetic properties. Previous study shows that, when exposed to a rotating DMF, the constant realignment of water molecules induces mechanical stress on their intermolecular hydrogen bonds [14]. This repetitive stress leads to "bond fatigue", weakening the structure of water molecules and facilitating easier dissociation into hydrogen and oxygen. The combined effects of ion mobility, reduced fouling, and water bond fatigue contribute to an overall increase in the efficiency of the HER process.

The large-scale design upgrades, including power capacity enhancement, material optimization, and improved mechanical elements, effectively addressed the limitations of the lab-scale system, ensuring that it meets industrial demands for efficiency, durability, and safety. The rotator power capacity was significantly increased from a small power of less than 100 W in the lab-scale to 12.5 MW in the large-scale design, as shown in Table 1. This scaling up was necessary to meet industrial demand and improve operational efficiency. The shift in rotator material, from standard steel to S30C carbon steel, was informed by a careful selection process based on working stress and durability. The shaft diameter was also increased from 50 mm to 95 mm, a decision that was essential to handle higher torque and stress loads (Table 1). Furthermore, the rotational speed was meticulously designed for 500 rpm in the new system, adapting to the requirements of the larger motor, whereas it was not carefully calculated in the lab-scale version. The improvement in allowable shear stress by using S30C carbon steel allowed for a higher load capacity, addressing material limitations of the previous design. In terms of mechanical elements, NA6917 needle roller bearings and M25 fixed couplings were introduced for durability and enhanced power transmission, contributing to system reliability under heavy loads (Table 1). The gear material was also upgraded to S45C carbon steel, chosen for its strength and wear resistance. Finally, the increase in the safety factor to greater than 1.5 and the system's ability to handle over 500 N·m of load demonstrate how the design improvements align with industrial scalability and safety requirements.

The practical implication of DMF utilization in HER is significant for electrolysis efficiency optimization. The enhancement of ion mobility and the mitigation of electrode fouling by DMF lead to higher and more consistent hydrogen production rates. The DMF-induced fatigue of water intermolecular bonds facilitates easier dissociation, which may further improve electrochemical water-splitting reaction efficiency. This approach not only boosts the performance of electrolysis systems but also extends the lifespan of electrodes. Consequently, the integration of DMF technology into large-scale hydrogen production systems can enhance overall hydrogen production efficiency, potentially reduce costs per volume of produced hydrogen, and support the advancement of green hydrogen solutions towards the NZE 2050 goal. It is also suitable to apply DMF in other practical areas of hydrogen production, including ammonia fertilizer production, medical applications of hydrogen, and other hydrogen production applications.

The key advantage of this study compared to existing solutions lies in its novel integration of a high-power DMF magnetic rotator design optimized for both efficiency and material durability, which is a significant improvement over conventional systems. While other designs focus primarily on scaling or material selection individually, this study uniquely combines both aspects by carefully selecting S30C and S45C carbon steels based on working stress and mechanical demands, along with precise engineering of load handling components such as bearings and couplings. Alternative solutions often overlook the detailed optimization of electron velocity targeting and magnetic field manipulation, which this study pioneers, allowing for enhanced electron spin alignment and improved water molecule manipulation in the electrolysis process. These specific features of material optimization, load capacity, and electron manipulation provide the advantages of increased power efficiency, scalability, and durability, setting this design apart from traditional approaches.

This work provides the design for a DMF magnetic rotator to be used in large-scale electrolyzers. However, this work does not include tests or simulations for stress distribution, cyclic loading, or shock testing due to various constraints such as time, resources, or scope limitations. Stress distribution simulations, typically performed using finite element analysis (FEA), are crucial for understanding how stress is distributed throughout the shaft under various loading conditions. FEA is a computational technique used to predict how a component or structure will respond to various forces, loads, and conditions by dividing it into smaller, simpler elements [53]. Cyclic loading tests evaluate the material's fatigue strength by subjecting it to repeated stress cycles, while shock tests assess the material's ability to withstand sudden, extreme loads [54]. The tests are important for validating the design and ensuring long-term reliability and safety. As a result, there may be unaccounted-for risks and potential failure points that only empirical testing could reveal, highlighting the need for further validation through comprehensive testing in future stages of the DMF magnetic rotator design.

The disadvantage of this work is related to the additional power required to run the whole electrolyzer's system. The SIEMENS Sylizer 300 requires 25 MW power and the motor to run the DMF magnetic rotator module as a booster requires half of it, which is 12.5 MW. The efficiency of the resulting hydrogen should be carefully noted in the future. The adaptive control of the magnetic rotator RPM is also required to maintain the power input since a greater load represents more energy input. Therefore, adjustable RPM of the magnetic motor according to the current efficiency is the possible development of this study.

7. Conclusions

1. The conceptual design of the magnetic rotator for the SIEMENS Sylizer 300 PEM electrolyzer effectively integrates the need for precise performance based on the electron density in the cathode. The design ensures that the chosen 12.5 MW, 14-pole induction motor meets the required operational parameters, such as load and rotational speed, while accounting for practical considerations and safety factors. This approach balances theoretical calculations with real-world

constraints, providing a robust solution that aligns with the specific needs of the electrolyzer system.

2. The determination of mechanical parts and interconnections for the DMF magnetic rotator, based on the conceptual design, effectively addresses the key engineering requirements. By calculating the allowable shear stress and verifying the shaft diameter, the design ensures that the shaft and spline can handle the applied torque and shock loads without exceeding material limits. The chosen 95 mm shaft diameter and selected spline dimensions meet the necessary criteria for safe operation. The spline dimension is l=80–320 mm and b=28 mm. The integration of standard components such as the clutch, gears, and bearings aligns with the design's need for power transmission and load handling. This thorough approach ensures that the mechanical parts and interconnections are suitably designed for the DMF magnetic rotator, balancing theoretical predictions with practical considerations to achieve reliable and efficient performance.

3. The design of the DMF magnetic rotator effectively incorporates the selection of mechanical elements based on allowable mechanical stresses. The choice of a 95 mm diameter S30C carbon steel shaft, strategically placed bearings, and splined interconnections ensures that the system can handle operational loads while maintaining structural integrity. The material selection for components such as the M25 fixed coupling, S45C carbon steel gears, and NA6917 needle roller bearings align with the requirements for strength and durability. The spline shear stress of 2.6 kg/mm^2 is still far below the allowable stress of 7.8 kg/mm^2. By applying the principles of maximum allowable stress and safety factors, the design balances theoretical calculations with practical considerations, ensuring reliable and efficient performance. This approach confirms that each component is suitably chosen to manage the mechanical stresses encountered in the system, providing a robust and dependable solution for the magnetic rotator.

Conflict of interest

The authors declare that they have no conflict of interest in relation to this research, whether financial, personal, authorship or otherwise, that could affect the research and its results presented in this paper.

Financing

This study is financially supported by Direktorat riset dan pengabdian masyarakat Universitas Brawijaya (DRPM UB) through Hibah Penelitian Pengembangan Unggulan (PPU) with grant No.[00147.2/UN10.A0501/B/PT.01.03.2/2024].

Data availability

Data will be made available on reasonable request.

Use of artificial intelligence

The authors confirm that they did not use artificial intelligence technologies when creating the current work.

Acknowledgments

We express our special gratitude to Universitas Brawijaya (DRPM UB) for their funding support. We also would like to thank the parties involved in this study, namely the Department of Mechanical Engineering, Universitas Brawijaya (UB), PT. Inti Dunia Energi Terbarukan (INERBA), and PT. Pilar dunia energi (PILAR) for their technical and administrative support.

References

1. Handayani, K., Krozer, Y., Filatova, T. (2017). Trade-offs between electrification and climate change mitigation: An analysis of the Java-Bali power system in Indonesia. Applied Energy, 208, 1020–1037. https://doi.org/10.1016/j.apenergy.2017.09.048
2. Arcos, J. M. M Santos, D. M. F. (2023). The Hydrogen Color Spectrum: Techno-Economic Analysis of the Available Technologies for Hydrogen Production. Gases, 3 (1), 25–46. https://doi.org/10.3390/gases3010002
3. Incer-Valverde, J., Korayem, A., Tsatsaronis, G., Morosuk, T. (2023). "Colors" of hydrogen: Definitions and carbon intensity. Energy Conversion and Management, 291, 117294. https://doi.org/10.1016/j.enconman.2023.117294
4. Energy Explained. The hydrogen colour spectrum. Available at: https://www.nationalgrid.com/stories/energy-explained/hydrogen-colour-spectrum
5. Diab, J., Fulcheri, L., Hessel, V., Rohani, V., Frenklach, M. (2022). Why turquoise hydrogen will Be a game changer for the energy transition. International Journal of Hydrogen Energy, 47 (61), 25831–25848. https://doi.org/10.1016/j.ijhydene.2022.05.299
6. Al-Douri, A., Groth, K. M. (2024). Hydrogen production via electrolysis: State-of-the-art and research needs in risk and reliability analysis. International Journal of Hydrogen Energy, 63, 775–785. https://doi.org/10.1016/j.ijhydene.2024.03.188
7. Grigoriev, S. A., Fateev, V. N., Bessarabov, D. G., Millet, P. (2020). Current status, research trends, and challenges in water electrolysis science and technology. International Journal of Hydrogen Energy, 45 (49), 26036–26058. https://doi.org/10.1016/j.ijhydene.2020.03.109
8. Schmitz, R., Brandes, J., Nolte, H., Kost, C., Lux, B., Haendel, M., Held, A. (2024). Implications of hydrogen import prices for the German energy system in a model-comparison experiment. International Journal of Hydrogen Energy, 63, 566–579. https://doi.org/10.1016/j.ijhydene.2024.03.210
9. Zainal, B. S., Ker, P. J., Mohamed, H., Ong, H. C., Fattah, I. M. R., Rahman, S. M. A. et al. (2024). Recent advancement and assessment of green hydrogen production technologies. Renewable and Sustainable Energy Reviews, 189, 113941. https://doi.org/10.1016/j.rser.2023.113941
10. Konyukhov, V. K. (2011). Spin states ofpara-water andortho-water molecule in gas and liquid phases. Physics and Chemistry of Liquids, 49 (3), 343–346. https://doi.org/10.1080/00319100903456154

11. Chen, Y.-J., Li, Y.-H., Chen, C.-Y. (2022). Studying the Effect of Electrode Material and Magnetic Field on Hydrogen Production Efficiency. Magnetochemistry, 8 (5), 53. https://doi.org/10.3390/magnetochemistry8050053
12. da Silva Falcão, B., Jeong, K., Al Ghafri, S., Robinson, N., Tang, L., Kozielski, K., Johns, M. L. (2024). Ortho- to para-hydrogen catalytic conversion kinetics. International Journal of Hydrogen Energy, 62, 345–351. https://doi.org/10.1016/j.ijhydene.2024.02.380
13. Purnami, P., Winarto, W., Sofi'i, Y. K., Nugroho, W. S., Wardana, I. N. G. (2023). The enhancement of magnetic field assisted water electrolysis hydrogen production from the compact disc recordable waste polycarbonate layer. International Journal of Hydrogen Energy, 48 (48), 18154–18165. https://doi.org/10.1016/j.ijhydene.2023.01.329
14. Purnami, P., Hamidi, N., Nur Sasongko, M., Siswanto, E., Widhiyanuriyawan, D., Pambudi Tama, I. et al. (2022). Enhancement of hydrogen production using dynamic magnetic field through water electrolysis. International Journal of Energy Research, 46 (6), 7309–7319. https://doi.org/10.1002/er.7638
15. Purnami, P., Satrio Nugroho, W., Hamidi, N., W, W., Schulze, A. A., Wardana, I. N. G. (2024). Double deep Q network intelligent adaptive control for highly efficient dynamic magnetic field assisted water electrolysis. International Journal of Hydrogen Energy, 59, 457–464. https://doi.org/10.1016/j.ijhydene.2024.01.321
16. Purnami, P., Satrio Nugroho, W., Sofi'i, Y. K., Wardana, I. N. G. (2024). The impact of sodium lauryl sulfate on hydrogen evolution reaction in water electrolysis. International Journal of Hydrogen Energy, 79, 1395–1405. https://doi.org/10.1016/j.ijhydene.2024.07.127
17. Purnami, P., Willy Satrio, N., Sofi'i, Y. K., Wardana, I. N. G. (2024). The impact of mechanical vibration at cathode on hydrogen yields in water electrolysis. Journal of Power Sources, 615, 235075. https://doi.org/10.1016/j.jpowsour.2024.235075
18. Handiwibowo, G. A., Nadlifatin, R., Bhawika, G. W., Noer, L. R. (2021). The Contribution of Absorptive Capacities to New Innovative Product Development Performance: A Conceptual Framework. International Journal of Mechanical Engineering Technologies and Applications, 2 (1), 73. https://doi.org/10.21776/mechta.2021.002.01.11
19. Setyarini, P. H., Gapsari, F., Harjo, A. O. R. (2022). Surface Characterization on Electrophoretic Deposition Oof 316l Stainless Steel with Dissolved Chitosan for Biomedical Application. International Journal of Mechanical Engineering Technologies and Applications, 3 (1), 40. https://doi.org/10.21776/mechta.2022.003.01.6
20. Juniansyah, G., Lathifah, S. M., Prajitno, D. H. (2021). Synthesis Polymer Matrix Composite Epoxy-FeNdB-Mn for Radar Absorbing Material Application. International Journal of Mechanical Engineering Technologies and Applications, 2 (1), 1. https://doi.org/10.21776/mechta.2021.002.01.1
21. Akbar, D. H., Purnami, P., Budio, S. P. (2020). Influence of Surface Roughness and Paint Coating on Corrosion Rate. International Journal of Mechanical Engineering Technologies and Applications, 1 (1), 15. https://doi.org/10.21776/mechta.2020.001.01.3
22. Habiby, M. N. A., Istianto, P. V., Fahmi, M. (2023). Optimization of cutting direction parameters for a cnc milling machining process pocket on structure and surface roughness on postep motorcycle spare parts. International Journal of Mechanical Engineering Technologies and Applications, 4 (2), 135–143. https://doi.org/10.21776/mechta.2023.004.02.3
23. Widodo, T. D., Raharjo, R., Risonarta, V. Y., Bintarto, R., Kusumaningsih, H., Saputra, M. H. (2020). The Effect of Sand Blasting on Shear Stress of Fiberglass – Shorea spp. Composite. International Journal of Mechanical Engineering Technologies and Applications, 1 (1), 1. https://doi.org/10.21776/mechta.2020.001.01.1
24. Anggamawarti, M. F., Alviari, L. P., Sanjiwani, Y., Risonarta, V. Y. (2020). Quality Analysis of 5.56 mm Ammunition Defect using Taguchi Method: A Review. International Journal of Mechanical Engineering Technologies and Applications, 1 (1), 29. https://doi.org/10.21776/mechta.2020.001.01.5
25. Ihsan, M. A., Sumantri, Y., Irawan, Y. S. (2024). Integration of taguchi and promethee for cnc milling machining parameter optimization on AA6061. International Journal of Mechanical Engineering Technologies and Applications, 5 (1), 96–107. https://doi.org/10.21776/mechta.2024.005.01.10
26. Flamm, B., Peter, C., Büchi, F. N., Lygeros, J. (2021). Electrolyzer modeling and real-time control for optimized production of hydrogen gas. Applied Energy, 281, 116031. https://doi.org/10.1016/j.apenergy.2020.116031
27. Ravichandran, S., Venkatkarthick, R., Sankari, A., Vasudevan, S., Jonas Davidson, D., Sozhan, G. (2014). Platinum deposition on the nafion membrane by impregnation reduction using nonionic surfactant for water electrolysis – An alternate approach. Energy, 68, 148–151. https://doi.org/10.1016/j.energy.2014.02.077
28. Xu, Y., Wang, C., Huang, Y., Fu, J. (2021). Recent advances in electrocatalysts for neutral and large-current-density water electrolysis. Nano Energy, 80, 105545. https://doi.org/10.1016/j.nanoen.2020.105545
29. Peter, C., Vrettos, E., Büchi, F. N. (2022). Polymer electrolyte membrane electrolyzer and fuel cell system characterization for power system frequency control. International Journal of Electrical Power & Energy Systems, 141, 108121. https://doi.org/10.1016/j.ijepes.2022.108121
30. Boichenko, S., Danilin, O., Shkilniuk, I., Yakovlieva, A., Khotian, A., Pavlovskyi, M. et al. (2023). Substantiating the expediency of using hydrogen fuel cells in electricity generation. Eastern-European Journal of Enterprise Technologies, 3 (8 (123)), 17–29. https://doi.org/10.15587/1729-4061.2023.280046
31. Mustafa, F. F., Hussein, O., Fakhri, O. F., Sabri, A. H. (2020). Design and development of high-accuracy machine for wire bending. Eastern-European Journal of Enterprise Technologies, 5 (1 (107)), 29–35. https://doi.org/10.15587/1729-4061.2020.202184
32. Lytvyn, V., Vysotska, V., Shatskykh, V., Kohut, I., Petruchenko, O., Dzyubyk, L. et al. (2019). Design of a recommendation system based on collaborative filtering and machine learning considering personal needs of the user. Eastern-European Journal of Enterprise Technologies, 4 (2 (100)), 6–28. https://doi.org/10.15587/1729-4061.2019.175507

33. Kvasnikov, V., Kvashuk, D., Prygara, M., Legeta, J. (2023). Designing tools for assessing the reliability of electric motor torque measurements by using identifiers of anomalous deviations in a noisy signal system. Eastern-European Journal of Enterprise Technologies, 6 (5 (126)), 15–25. https://doi.org/10.15587/1729-4061.2023.292187
34. Suga, K., Sularso (1997). Dasar Perencanaan dan Pemilihan Elemen Mesin. Jakarta: Pradnya Paramitha.
35. Nanda, R. A., Karyadi, K., Roban, R., Dewadi, F. M. (2024). RPM measurement comparison using a thermometer and LM393 microcontroller. International Journal of Mechanical Engineering Technologies and Applications, 5 (1), 51–62. https://doi.org/10.21776/mechta.2024.005.01.6
36. Kvasnikov, V., Kvashuk, D., Prygara, M., Shelukha, O., Molchanova, K. (2024). Devising a technique for measuring torque of electric motors using machine vision. Eastern-European Journal of Enterprise Technologies, 1 (5 (127)), 16–32. https://doi.org/10.15587/1729-4061.2024.298513
37. Darmo, S., Soenoko, R., Siswanto, E., Widodo, T. D. (2019). The influence of the pack decarburizing process with Pinctada maxima shell powder agent on the properties of high carbon steel. Eastern-European Journal of Enterprise Technologies, 1 (12 (97)), 6–13. https://doi.org/10.15587/1729-4061.2019.153762
38. Xu, H., Wang, P., Ma, H., He, D., Zhao, X., Yang, Y. (2022). Analysis of axial and overturning ultimate load-bearing capacities of deep groove ball bearings under combined loads and arbitrary rotation speed. Mechanism and Machine Theory, 169, 104665. https://doi.org/10.1016/j.mechmachtheory.2021.104665
39. Huang, W., Tian, H., Ma, H., Wang, P., Yang, Y., Han, Q. (2023). An improved method for calculating the lateral and angular stiffness of spline couplings considering parallel misalignment. Mechanism and Machine Theory, 189, 105436. https://doi.org/10.1016/j.mechmachtheory.2023.105436
40. Morozyuk, L., Hrudka, B., Yuzhakova, O. (2018). Selection of new working fluids for a heat-using compression refrigerating machine with the block "turbine-compressor". Eastern-European Journal of Enterprise Technologies, 5 (8 (95)), 33–40. https://doi.org/10.15587/1729-4061.2018.142061
41. Yurianto, Y., Pratikto, P., Soenoko, R., Suprapto, W. (2019). Effect of quench and temper on hardness and wear of HRP steel (armor steel candidate). Eastern-European Journal of Enterprise Technologies, 3 (12 (99)), 55–61. https://doi.org/10.15587/1729-4061.2019.156799
42. Rahman, A., Winarto, W., Siswanto, E. (2024). Optimization of shell and tube heat exchanger design with inclined baffles. International Journal of Mechanical Engineering Technologies and Applications, 5 (1), 63–72. https://doi.org/10.21776/mechta.2024.005.01.7
43. Sugiono, S., Nugroho, W. S., Wiryawan, E., Oktavianty, O., Sulistyarini, D. H. (2023). Controlling the train car's center of gravity (COG) position based on train load levelling. Journal of Applied Research and Technology, 21 (6), 1057–1065. https://doi.org/10.22201/icat.24486736e.2023.21.6.1977
44. Quan, Z., Ge, L., Wei, Z., Li, Y. W., Quan, L. (2021). A Survey of Powertrain Technologies for Energy-Efficient Heavy-Duty Machinery. Proceedings of the IEEE, 109 (3), 279–308. https://doi.org/10.1109/jproc.2021.3051555
45. de Souza, D. F., Salotti, F. A. M., Sauer, I. L., Tatizawa, H., de Almeida, A. T., Kanashiro, A. G. (2022). A Performance Evaluation of Three-Phase Induction Electric Motors between 1945 and 2020. Energies, 15 (6), 2002. https://doi.org/10.3390/en15062002
46. Sutrisno, S., Soenoko, R., Irawan, Y. S., Widodo, T. D. (2021). Effect of coconut fiber treatment with limestone water media on the fiber surface, wettability, and interface shear strength. Eastern-European Journal of Enterprise Technologies, 1 (6 (109)), 48–56. https://doi.org/10.15587/1729-4061.2021.217730
47. Taufik, A., Pratikto, P., Suprapto, A., Sonief, A. A. (2021). Analysis of the influence of hot rolled plate steel treatment using temper and quench-temper method on vickers hardness number enhancement. Eastern-European Journal of Enterprise Technologies, 4 (12 (112)), 18–24. https://doi.org/10.15587/1729-4061.2021.233349
48. Soenoko, R., Purnami, Utami Dewi, F. G. (2017). Second stage cross flow turbine performance. ARPN Journal of Engineering and Applied Sciences, 12 (6). Available at: http://www.arpnjournals.org/jeas/research_papers/rp_2017/jeas_0317_5818.pdf
49. Sugiarto, S., Soenoko, R., Purnowidodo, A., Irawan, Y. S. (2018). The effect of external magnetic flux field in the QTS weldment on the change of fatigue crack propagation behaviors. Eastern-European Journal of Enterprise Technologies, 2 (12 (92)), 4–11. https://doi.org/10.15587/1729-4061.2018.122919
50. Sugiarto, Purnowidodo, A., Soenoko, R., Irawan, Y. S., Sonief, A. A. (2016). The use of magnetic flux to the welding of hot roll quench tempered steel. ARPN Journal of Engineering and Applied Sciences, 11 (2), 1061–1064. Available at: http://www.arpnjournals.org/jeas/research_papers/rp_2016/jeas_0116_3454.pdf
51. Sugiarto, Dr., Ma'arif, Moch. S., Purwanto, H., Ery Mahendra, W. J., Oswari, H. (2023). Characteristic of friction stir welding weld joint of AA 6061 on initial temperature difference. MM Science Journal, 2023 (1). https://doi.org/10.17973/mmsj.2023_03_2022094
52. Wijayanti, W., Sasongko, M. N., Purnami (2016). The calorific values of solid and liquid yields consequenced by temperatures of mahogany pyrolysis. ARPN Journal of Engineering and Applied Sciences, 11 (2), 917–921. Available at: http://www.arpnjournals.org/jeas/research_papers/rp_2016/jeas_0116_3427.pdf
53. Sunardi, Choiron, Moch. A., Sugiarto, Setyarini, P. H. (2023). Development of fishing boat collision models in extreme weather using computer simulation. EUREKA: Physics and Engineering, 2, 149–159. https://doi.org/10.21303/2461-4262.2023.002601
54. Sunardi, E. F., Choiron, M. A., Sugiarto, A. W. M., Setyarini, P. H., Nurwahyudi, A. (2024). Fishing Vessel Safety in Indonesia: A Study of Accident Characteristics and Prevention Strategies. International Journal of Safety and Security Engineering, 14 (2), 499–511. https://doi.org/10.18280/ijsse.140217